Phys. Status Solidi B, 1–4 (2009) / **DOI** 10.1002/pssb.200982254

physica status solidi b
www.pss-b.com
basic solid state physics

Boron, nitrogen and phosphorous substitutionally doped single-wall carbon nanotubes studied by resonance Raman spectroscopy

I. O. Maciel[*,1], J. Campos-Delgado[2], M. A. Pimenta[1], M. Terrones[2], H. Terrones[2], A. M. Rao[3], and A. Jorio[1,4]

[1] Departamento de Física, Universidade Federal de Minas Gerais, Belo Horizonte, MG, 30123-970 Brazil
[2] Advanced Materials Department, IPICYT, San Luis Potosí, SLP, 78216, Mexico
[3] Department of Physics and Astronomy, Clemson University, Clemson, South Carolina 29634, USA
[4] Divisão de Metrologia de Materiais, Instituto Nacional de Metrologia, Normalização e Qualidade Industrial (INMETRO), Duque de Caxias, RJ, 25250-020, Brazil

Received 20 April 2009, revised 2 July 2009, accepted 14 August 2009
Published online 16 October 2009

PACS 73.20.Hb, 73.22.–f, 78.30.Na, 78.67.Ch

[*] Corresponding author: e-mail indhira@fisica.ufmg.br, Phone: +55-31-3409-6610, Fax: 55+31-3409-5600

Substitutional doping on single-wall an on multi-wall carbon nanotubes is possible by adding new atoms during the growing process. In this work we analyze the changes in the Raman spectra of SWNT samples substitutionaly doped with boron, nitrogen, and phosphorous. We find that small amounts of dopants are not enough to change the frequency of the tangential G mode, but there is a doping-dependent shift in ω_G when the P-doped SWNTs are measured at high laser power, indicating that doping can change the thermal properties of SWNT bundles. This result seems to hold also for B-doped samples, but not for N-doped SWNTs, showing a different behavior for donors (P- and N- doping). The I_D/I_G ratio analysis to provide information about the doping level in the SWNT samples is also discussed.

1 Introduction Doping single-wall (SWNTs) and multi-wall (MWNTs) carbon nanotubes induce changes in the tubes properties [1]. Most of the substitutionally doped SWNTs contain less than 1% of dopants, making it difficult to identify and characterize these samples with most of the techniques, such as electron diffraction and high resolution electron beam microscopy [1, 2]. For MWNT samples, the amount of dopants can be detected by energy dispersive X-ray spectroscopy (EDX) or energy electron loss spectroscopy (EELS) [2, 3] because these many layered tubes can support more doping atoms. In the case of SWNTs, larger amount of doping increases disorder or even stop the nanotube growth [2, 4], making it harder to identify the realistic content of dopants, and thus requiring systematic studies on SWNT growth to detect dopants in good quality samples [5, 6].

It was demonstrated that SWNTs can be doped with boron (B) [4, 7], nitrogen (N), [2] or phosphorous (P) [3, 8] atoms. B is an electron acceptor to NTs, N, and P are electron donors, the nature (local vs. non-local) of electron doping of N and P being different. First principle calculations show that while the N atom lies on the plane of the nanotube lattice, P is attached to the tube with three sp^2-like bonds to the C neighbor atoms, laying out of the plane of the nanotube [3, 9].

The frequency shift in the first-order Raman tangential G band feature has been used to study doping [10–12]. In this work we study the ω_G shifts in different doped samples. We find, for the measured samples, that there is no frequency shift in ω_{G+} due to doping, except when the measurements are taken at high laser power, indicating that doping induces changes in the heat transfer of the bundled nanotubes. Furthermore, we analyze the I_D/I_G ratio to infer the doping level of the SWNT samples, discussing the accuracy of this method.

2 Experimental details Boron-doped SWNTs were grown by the pulsed laser vaporization technique using targets with three different boron concentrations, i.e. undoped, 1.5 at.% and 3.0 at.% [4]. Nitrogen and phosphorous doped samples were grown by chemical vapor deposition (CVD) at 950 °C using a solution of ethanol with 1.25% in weight of ferrocene as a precursor, carried by a

1.2 l/min flux of argon for N samples and 0.8 l/min flux of argon–hydrogen gas mixture (5% of hydrogen) for 30 min [8]. The N doping was achieved by adding benzilamine in the precursor solution in the following concentrations: 0, 3.0, 7.0, and 11.0% in weight. For the phosphorous doping, triphenilphosphine was added to the ferrocene solution in the following concentrations: 0, 0.1, 0.15, 0.2, and 0.25% in weight [8]. The samples will be labeled in this discussion by the precursor solution concentrations used in the growing process.

Resonance Raman spectroscopy measurements were performed with a Dilor XY triple-monochromator with an 80× objective in a backscattering configuration. The apparatus is equipped with CCD detectors and the excitation came from an ArKr laser with the 2.41 eV (514.5 nm) energy.

3 Results and discussion The initial characterization of the samples was made by measuring the tangential G band mode and the disorder-induced D band. The G band is composed of two prominent peaks, here named G^+ and G^- for the higher and the lower frequency peaks, respectively. Figure 1 shows these bands measured with 2.41 eV excitation energy and 0.2 mW laser power at low laser power (< 0.2 mW), the position of the most intense G^+ peaks are 1592, 1594, and 1594 cm^{-1} for the B, N, and P samples, respectively, independently of the doping level. Therefore, at low laser power, the amount of dopants is not enough to cause any change in the SWNTs tangential mode frequencies.

When the samples are measured with the same excitation energy and high laser powers (2.0 mW), redshifts in the ω_{G^+} position are observed, depending on the dopant type and their percentages. High laser power heats the samples and there is a general phonon softening. The fact that the redshift in ω_{G^+} depends on the dopant type and their percentages means that doping is changing the thermal transport in the samples. Figure 2 shows the ω_{G^+} shift for the samples measured at 2.0 mW compared to measurements made at 0.2 mW, i.e., $(\omega_{G^+_{P=2.0\ mW}} - \omega_{G^+_{P=0.2\ mW}})$. In the case of boron, the 1.5 at.% doped sample has an overall smaller redshift, which means that B is increasing the heat dissipation of the sample. For the 3.0 at.% B doped sample, the sample is already too defective, mostly composed of amorphous carbon, as can be inferred by the I_D/I_G ratio around 0.4 (see Fig. 1(a)). The heat dissipation can then be compromised. It also happens that the ω_G frequency of amorphous carbon is smaller than ω_{G^+} of nanotubes, meaning that the average G peak seen in the Raman spectra of the 3.0 at.% sample can come from both materials, making the analysis of the 3.0 at.% B sample meaningless. For the N-doped samples, an homogeneous redshift is observed, independent of the doping level, as can be seen in Fig. 2(b). In the case of P, the increase of doping level clearly increases the heat dissipation, as can be seen from the smaller redshifts in Fig. 2(c) with increasing doping.

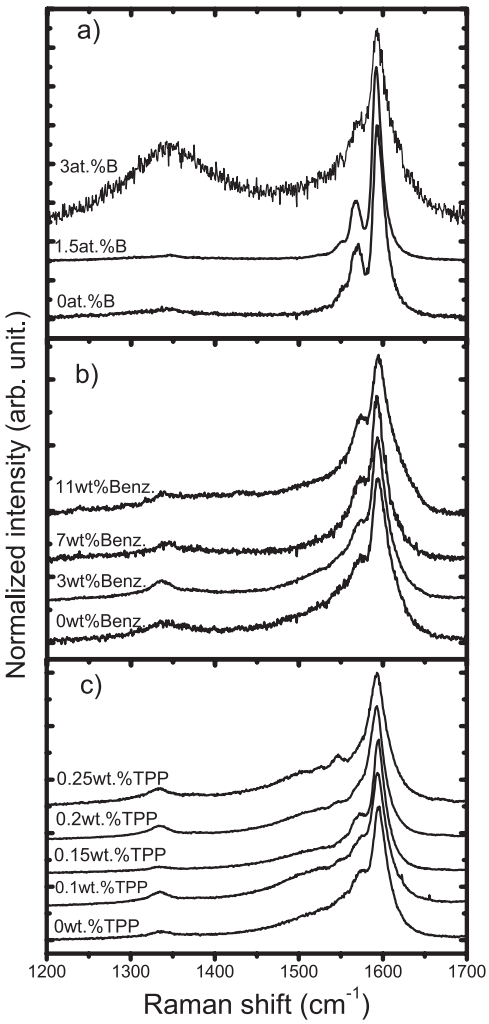

Figure 1 D and G bands for (a) B-, (b) N-, and (c) P-doped SWNT samples for different doping concentrations. No shift in the ω_G frequency is observed as intrinsically due to structural changes caused by doping. The I_D/I_G ratio is smaller than 0.2, except in the 3.0 at.% B-doped sample, where $I_D/I_G \sim 0.4$. The laser excitation energy is 2.41 eV.

To clarify the effect of B-doping evidenced by Fig. 2 (a), Fig. 3 shows the dependence of ω_{G^+} with laser power for the undoped and the 1.5 at% B-doped samples. The temperature dependence of ω_{G^+} is found to be linear for high pressure carbon monoxide (HIPCO) SWNT bundles [13]. Considering that the ω_{G^+} dependence with laser power is also linear, fits to the linear portion of the data can be given by the equation:

$$\omega_{G(P)} = \omega_{G^+_0} + cP, \quad (1)$$

where P is the laser power in mW and c is a constant. Table 1 gives the values of $\omega_{G^+_0}$ and c for the two samples. These fits are applicable up to ~3 mW. At higher laser power, there is a saturation behavior in ω_{G^+}. The value of c in Table 1 is

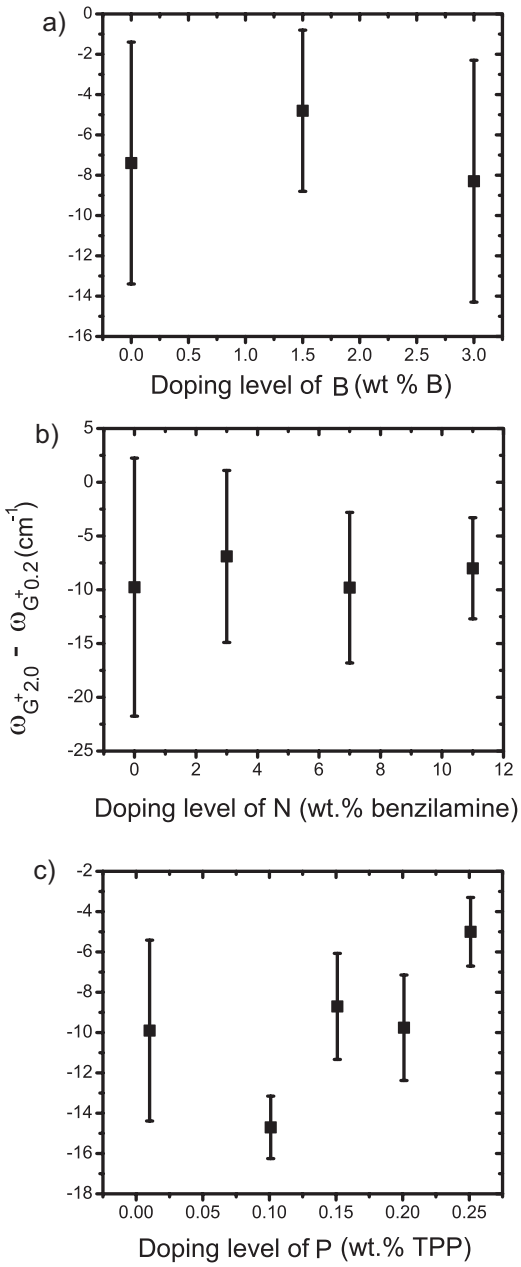

Figure 2 The G^+ band downshift ($\omega_{G^+_{P=2.0mW}} - \omega_{G^+_{P=0.2mW}}$) of (a) B-, (b) N- and (c) P-doped samples due to laser heating. The values of the G^+ band frequency were calculated by averaging the ω_{G^+} values in four different locations in the samples. The error bars indicate the spread over these measurements. Notice that the error bars are smaller with increasing doping (except for the 3.0 at.% B sample), meaning that the samples are more homogeneous with increasing doping.

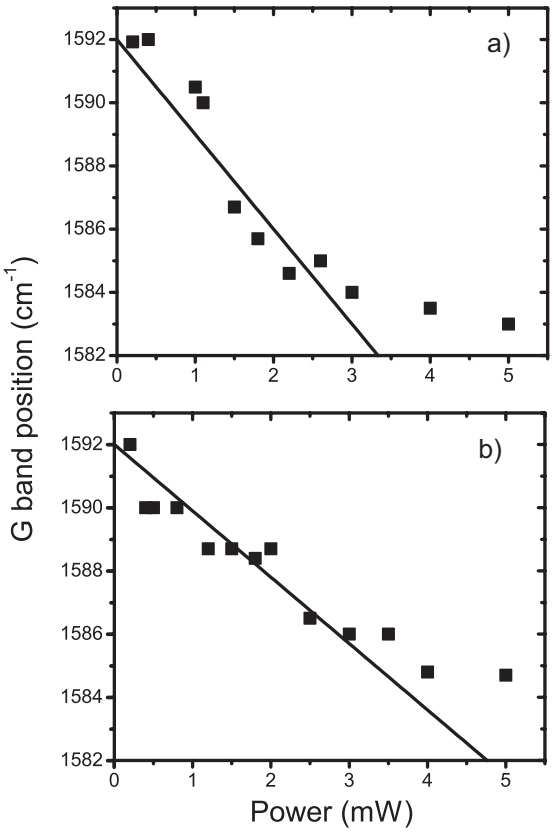

Figure 3 ω_{G^+} dependence with laser power for the (a) 0 at.% and (b) 1.5 at.% B-doped samples. The lines are linear fittings to the data up to ~3 mW, corresponding to the Eq. (1), with the parameters given in Table 1.

smaller for the 1.5 at.% B-doped sample, i.e., the shift in ω_{G^+} is smaller for this sample with increasing power. The saturation value of ω_{G^+} is also larger for the doped sample when compared to the undoped one, confirming that doping increases the thermal transport efficiency in the bundled samples. In a single nanotube, the scattering caused by a defect should cause a decrease of thermal conductivity. As our samples are in bundles, the scattering centers (doping atoms) are responsible to transfer heat from one nanotube to another, explaining the results shown here.

Finally, the I_D/I_G ratio is analyzed. The I_D/I_G is always smaller than 0.2, except for the 3.0 at.% B sample, as shown in Fig. 4. This shows that the crystallinity of the samples were not highly affected by doping, except for the 3.0 at.% B sample. The I_D/I_G ratio shows an overall increase with increasing doping level, but this increase is not enough to make the I_D/I_G analysis an accurate method to sense doping, since it can be related to other types of defects and amorphous carbon in the samples.

Table 1 Parameters for Eq. 1. $\omega_{G^+_0}$ are fixed at the frequency observed in the $P = 0.2$ mW measurements.

Doping level	$\omega_{G^+_0}$ (cm^{-1})	c(cm^{-1}/mW)
0 at.% B	(1592)	$-(3.0 \pm 0.2)$
1.5 at.% B	(1592)	$-(2.1 \pm 0.2)$

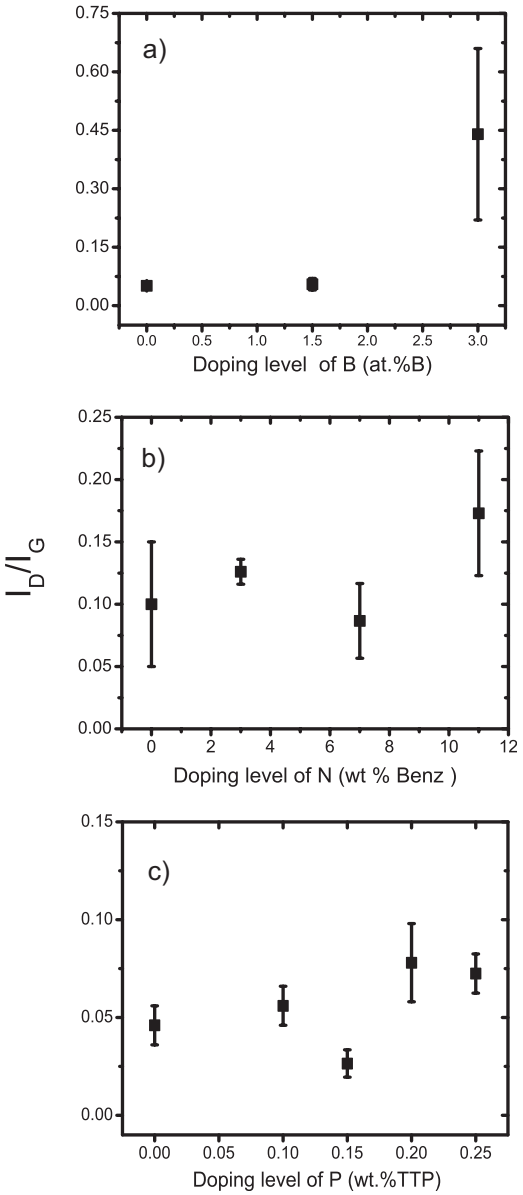

Figure 4 I_D/I_G ratios for (a) B-, (b) N- and (c) P-doped SWNT samples measured with 2.41 eV excitation energy. The values of the I_D/I_G ratios were calculated by averaging the values from four different locations in the samples. The error bars indicate the spread over these measurements.

4 Conclusions In this work we studied substitutionally doped SWNTs with of B, N, and P atoms, using resonance Raman spectroscopy. We showed that the small amounts of dopants in the samples are not able to shift the G band frequency. The ω_G frequency shifts only when the measurements are taken at high laser powers. For B and P cases, the redshift due to laser heating is smaller when the amount of doping atoms increases, showing an increase in thermal conductance for the bundled doped SWNTs. This result is not observed for N-doped samples, suggesting differences in the doping induced effects. We also showed that the I_D/I_G ratio shows an overall increase with increasing doping level. However, care should be taken since the D band intensity develops with any type of defect, including amorphous carbon.

Acknowledgements I. O. M., M. A. P. and A. J. acknowledge financial support from FAPEMIG, Rede Nacional de Pesquisa em Nanotubos de Carbono, Rede National de SPM and Instituto de Nanotecnologia (MCT-CNPq). M. T., H. T., and J. C-D acknowledge financial support from CONACYT-Mexico Grants No. 56787 (Laboratory for Nanoscience and Nanotechnology Research-LINAN), 45762 (HT), 45772 (MT), Fondo Mixto de San Luis Potosí 63001 S-3908 (MT), 2004-01-013/SALUD-CONACYT (MT), Fondo Mixto de San Luis Potosí 63072 S-3909 (HT), 58899-Inter American Collaboration, and PhD scholarship (JCD).

References

[1] A. Jorio, M. S. Dresselhaus, and G. Dresselhaus, Doped Carbon Nanotubes: Synthesis, Characterization and Applications, in: Carbon Nanotubes: Advanced Topics in the Synthesis, Structure, Properties and Applications, edited by M. Terrones, A. G. Souza Filho, and A. M. Rao, Vol. 111, Springer Ser. Topics in Appl. Phys. (Springer-Verlag, Berlin, 2008), p. 531.
[2] F. Villapando-Paez, A. Zamudio, A. L. Elias, H. Son, E. B. Barros, S. G. Chow, Y. A. Kim, H. Muramatsu, T. Hayashi, J. Kong, H. Terrones, G. Dresselhaus, M. Endo, M. Terrones, and M. S. Dresselhaus, Chem. Phys. Lett. **424**, 345 (2006).
[3] E. Cruz-Silva, D. A. Cullen, L. Gu, J. M. Romo-Herrera, E. Muoz-Sandoval, F. Lopez-Uras, B. G. Sumpter, V. Meunier, J.-C. Charlier, D. J. Smith, H. Terrones, and M. Terrones, ACSNANO **2**, 441 (2008).
[4] K. McGuire, N. Gothard, P. L. Gai, M. S. Dresselhaus, G. Sumanasekera, and A. M. Rao, Carbon **43**, 219 (2005).
[5] J. L. Blackburn, Y. Yan, C. Engtrakul, P. A. Parilla, K. Jones, T. Gennet, A. C. Dilon, and M. S. Heben, Chem. Mater. **18**, 2558 (2006).
[6] P. Alaya, M. H. Rmmeli, E. Kauppinen, H. Kuzmany, and T. Pichler, Phys. Status Solidi B **245**, 1935 (2008).
[7] P. L. Gai, O. Stephan, K. McGuire, A. M. Rao, M. S. Dresselhaus, G. Dresselhaus, and C. Colliex, J. Mater. Chem. **14**, 669 (2004).
[8] I. O. Maciel, N. Anderson, M. A. Pimenta, A. Hartschuh, H. Qian, M. Terrones, H. Terrones, J. Campos-Delgado, A. M. Rao, L. Novotny, and A. Jorio, Nat. Mater. **7**, 878 (2008).
[9] B. G. Sumpter, J. Huang, V. Meunier, J. M. Romo-Herrera, E. Cruz-Silva, H. terrones, and M. Terrones, Int. J. Quantum Chem. **109**, 97 (2009).
[10] A. M. Rao, P. C. Eklund, S. Bandow, A. Thess, and R. E. Smalley, Nature **388**, 257 (1997).
[11] J. C. Tsang, M. Freitag, V. Perebeinos, J. Liu, and Ph. Avouris, Nat. Nanotech. **2**, 725 (2007).
[12] A. G. Souza Filho, A. Jorio, Ge, G. Samsonidze, G. Dresselhaus, R. Saito, and M. S. Dresselhaus, Nanotechnology **14**, 1130 (2003).
[13] N. R. Raravikar, P. Keblinski, A. M. Rao, M. S. Dresselhaus, L. S. Schadler, and P. M. Ajayan, Phys. Rev. B **66**, 235424 (2002).

